applied sciences

MDPI

Article

Size- and Structure-Related Effects of Carbon Nanotubes on the Performance of Phase Change Materials for Thermal Energy Storage

Beata Macherzyńska, Adrianna Pitera, Julia Pakosz, Martyna Sioła and Kinga Pielichowska *

Department of Glass Technology and Amorphous Coatings, Faculty of Materials Science and Ceramics, AGH University of Krakow, Al. Mickiewicza 30, 30-059 Krakow, Poland; beatam@agh.edu.pl (B.M.); apitera@student.agh.edu.pl (A.P.); juliapakosz@student.agh.edu.pl (J.P.); szatkowska@agh.edu.pl (M.S.)
* Correspondence: kingapie@agh.edu.pl

Abstract

Phase change materials (PCMs) are a widely used group of materials for thermal energy storage; however, their practical applications are often limited by low thermal conductivity. Modification with carbon nanotubes (CNTs) as effective nanofillers can enhance not only the thermal performance of PCMs but also their ability for photothermal conversion. However, the influence of their dimensions and structure on the overall properties of PCM composites remains insufficiently understood. In this study, the effect of functionalized carbon nanotube size and structure on the thermal and functional properties of CNT-enhanced organic phase change materials was systematically investigated. Nanocomposite PCMs containing carbon nanotubes with different characteristics were prepared and comprehensively characterized using differential scanning calorimetry (DSC), thermogravimetric analysis (TGA), and Fourier transform infrared spectroscopy (FTIR). The long-term durability of the composites was evaluated through repeated heating–cooling cycles followed by thermal characterization to evaluate the stability of their energy storage performance. The photothermal conversion capability of the materials under a solar simulator was investigated, and microscopic observations were conducted to analyze the dispersion of carbon nanotubes and the morphology of the PCM nanocomposites. The results demonstrate that appropriate selection of CNT size improves thermal stability, preserves latent heat storage capacity during repeated thermal cycling, enhances photothermal conversion efficiency, and promotes a more homogeneous microstructure. The findings provide new insights into the design of high-performance PCM composites for advanced thermal energy storage and solar thermal energy harvesting applications.

Keywords: phase change materials; thermal energy storage; carbon nanotubes

Check for updates

Academic Editor: Yoong Ahm Kim

Received: 15 August 2026
Revised: 23 October 2026
Accepted: 26 October 2026
Published: 30 October 2026

Copyright: © 2026 by the authors. Licensee MDPI, Basel, Switzerland. This article is an open access article distributed under the terms and conditions of the Creative Commons Attribution (CC BY) license.

1. Introduction

Phase change materials (PCMs) represent a highly attractive and promising class of materials for efficient thermal energy storage. Their operation is based on their ability to absorb, store, and release large amounts of heat, referred to as latent heat, during reversible phase transitions, among which the solid–liquid transition is the most widely utilized [1–3]. Owing to their ability to maintain a constant or nearly constant temperature during the phase transition, PCMs have found broad application in numerous fields where balancing fluctuations between energy supply and demand is of critical importance. They are widely employed in the building sector to improve thermal comfort and temperature regulation, as

well as in solar energy systems, waste heat recovery, refrigeration, thermal management of electronic devices and batteries, and smart textiles. Their applications also extend to the food and biomedical industries [4–6].

In general classification, PCMs are categorized into organic, inorganic, and eutectic materials [7]. Inorganic PCMs, such as salt hydrates, generally exhibit higher thermal conductivity than their organic counterparts; however, they are often associated with several limitations, including corrosion, supercooling, and phase separation [8]. Organic phase change materials are characterized by high chemical stability, non-corrosive behavior, non-toxicity, and a broad range of phase transition temperatures [9]. Among organic PCMs, fatty acids constitute a particularly important and extensively investigated group [10,11]. These bio-based materials can be derived from both plant and animal sources and exhibit several advantageous properties, including favorable thermal characteristics, high heat storage capacity, low or negligible supercooling, and low vapor pressure [12]. Nevertheless, despite these numerous advantages, the primary limitation of fatty acids, like all organic PCMs, is their low thermal conductivity (typically on the order of 0.1–0.3 W/m·K), which slows down heat transfer processes and prolongs the charging and discharging cycles of thermal energy storage units [13]. To overcome this limitation and enhance heat transfer within the PCM, one of the most commonly employed approaches is the incorporation of thermally conductive nano-additives into the pristine phase change material [14–16]. In this context, carbon-based materials, including carbon nanotubes (CNTs), have attracted research interest due to their outstanding thermal and structural properties [17]. The incorporation of CNTs into a PCM matrix can promote the formation of thermally conductive pathways, thereby enhancing the effective thermal conductivity of the composite and improving its thermal response [18]. However, the introduction of nanoparticles may also affect other important properties of the PCM. In particular, the addition of CNTs may result in a certain reduction in the latent heat (enthalpy) of the phase transition. This decrease may be attributed, among other factors, to the replacement of a fraction of the active PCM by the nano-additive, which reduces the mass fraction of the phase-changing component in the composite. Furthermore, the presence of CNTs may introduce steric constraints or interfere with the molecular arrangement of the organic chains, potentially limiting the extent of crystallization [19]. Nevertheless, appropriate optimization of the type and concentration of the nano-additive can provide a favorable balance between enhanced thermal conductivity and an acceptable reduction in heat storage capacity [20].

The modification of PCMs with CNTs generally leads to improvements in selected properties. However, a review of the literature indicates that the reported effects vary considerably. One possible explanation for these discrepancies is the size of the incorporated CNTs. Therefore, the objective and novelty of this study lie in providing a comprehensive analysis of the selected properties of a fatty acid-based PCM modified with CNTs characterized by three different outer diameter ranges (7–16 nm, 18–38 nm, and 48–78 nm) and different characteristics at mass concentrations ranging from 0 to 2 wt.% (0, 0.25, 0.5, 1, and 2 wt.%). The results enable an assessment of the effects of CNT size and concentration on the key thermophysical properties of the resulting composites, including phase transition temperatures and enthalpies and material stability. The findings provide insights into the relationships between CNT characteristics, their concentration, and the resulting thermal performance of the PCM composites, thereby contributing to the development of optimized materials for advanced thermal energy storage and energy conversion applications.

2. Materials and Methods

Composite samples were prepared using RT80HC phase change material (PCM) supplied by Rubitherm Technologies GmbH, Berlin, Germany and industrial multi-walled

carbon nanotubes (CNTs) functionalized with hydroxyl (-OH) groups—with a purity of >92%—supplied by Nanografi Nano Teknoloji A.Ş., Jena, Germany. Three CNT fractions with different outer diameter ranges were used: 7–16 nm (CNT I), 18–38 nm (CNT II), and 48–78 nm (CNT III). The degree of functionalization was 2.5 wt.% for CNT I and II and 0.75 wt.% for CNT III—Table 1.

Table 1. Characteristics of the nanotubes used.

Parameters	Units	CNT_I	CNT_II	CNT_III
Purity	%		>92	
Content of (-OH)	wt.%	2.5	2.5	0.75
Outside Diameter	nm	7–16	18–38	48–78
Length	mm	30–50	10–35	10–30
SSA	m^2/g	260	120	50
Content of (-OH)/SA	g/m^2	0.096×10^{-3}	0.208×10^{-3}	0.15×10^{-3}

For the preparation of the composites, the required amount of PCM was weighed into glass vials and subsequently heated to 80 °C. The samples were maintained at this temperature until the PCM was completely melted. Subsequently, an appropriate amount of carbon nanotubes (CNTs) was gradually added to the molten PCM so that their concentration in the composite was 0.25, 0.5, 1, and 2 wt.%. During the addition of CNTs, the mixture was simultaneously homogenized using an ultrasonic homogenizer for 30 s to promote uniform dispersion of the nanofiller throughout the PCM matrix. The preparation procedure and the nomenclature adopted for the resulting composite materials are presented schematically in Figure 1. To assess the thermal stability of the composites, selected samples were subjected to 20 consecutive melting–solidification cycles. The melting stage was performed at 80 °C, whereas solidification was carried out at room temperature. The cycling tests were conducted under two different atmospheres: air and nitrogen.

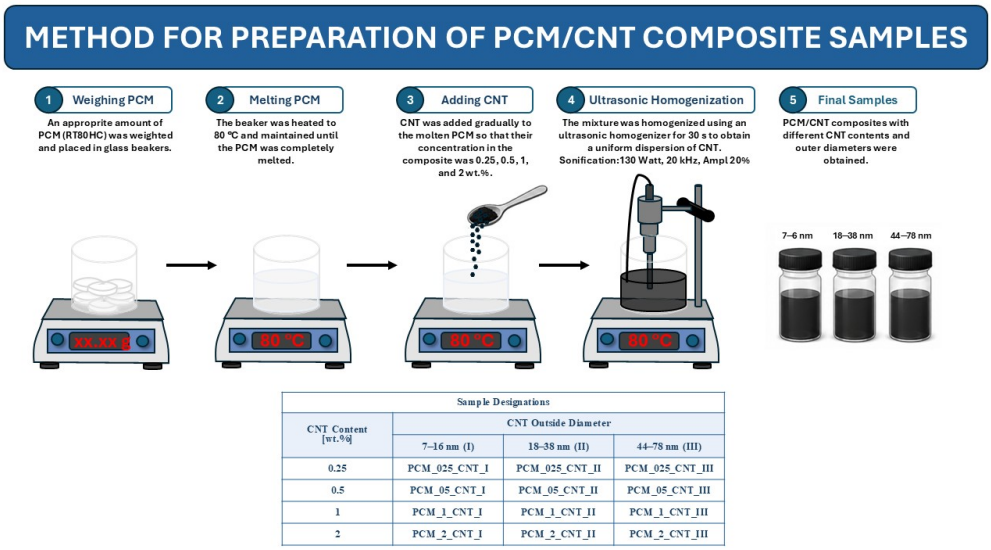


Figure 1. Schematic illustration of the preparation procedure for PCM/CNT composites. Source: ChatGPT (GPT-6, OpenAI) adapted and modified by the author.

Differential scanning calorimetry (DSC) measurements were performed using a DSC250 apparatus (TA Instruments, New Castle, DE, USA). A temperature program consisting of heating–cooling–heating cycles in the range from 20 to 110 °C was applied at a constant rate of 10 °C/min under a nitrogen atmosphere (340 mL/min). Samples with a

mass of approximately 3 mg were sealed in aluminum pans. To eliminate the influence of thermal history, the results of the second heating cycle were used for analysis. Additionally, DSC measurements under the same conditions were carried out for all materials after 20 melting/solidification cycles.

The degree of supercooling (ΔT) was determined according to Equation (1):

$$\Delta T = T_m - T_c \quad (1)$$

where T_m is the maximum melting temperature and T_c is the maximum crystallization temperature.

Furthermore, multi-frequency temperature modulation DSC measurements were performed in TOPEM mode using a DSC 1 (Mettler Toledo, Greifensee, Switzerland). Samples weighing approximately 10 mg were sealed in aluminum crucibles and, prior to measurements, were remelted at a heating rate of 20 °C/min and a cooling rate of 10 °C/min. The experiments were then conducted at a heating and cooling rate of 1 °C/min with a temperature modulation amplitude of 0.5 °C and a switching time of 15 s, over a temperature range of 20 to 110 °C, under a nitrogen atmosphere (30 mL/min). Thermogravimetric analysis (TGA) was performed using a TGA 550 Discovery analyzer from TA Instruments (New Castle, DE, USA). Samples weighing approximately 4 mg were placed in platinum crucibles and heated over a temperature range of 35 to 600 °C at a constant rate of 10 °C/min, under a nitrogen atmosphere. Fourier transform infrared spectroscopy (FTIR) measurements were obtained using a Thermo Scientific Nicolet Apex FTIR spectrophotometer (ThermoFisher Scientific, Waltham, MA, USA). Samples were scanned from 4000 to 600 cm^{-1}, and functional groups were identified by ATR after 32 scans at 4 cm^{-1}. Scanning electron microscopy (SEM) was performed using a NOVA NANO SEM 200 system (FEI, Hillsboro, OR, USA) equipped with EDS. Before imaging, the sample was coated with a carbon layer and examined at approximately 5000× magnification. Photothermal conversion efficiency was evaluated using an Ossila LED Solar Simulator (Ossila, Sheffield, UK) at room temperature over a period of 40 min. Following irradiation, the samples were placed in a custom-designed experimental setup for the assessment of their photothermal conversion performance, as described in [21,22]. A schematic diagram of the experiment and key parameters is shown in Figure 2.

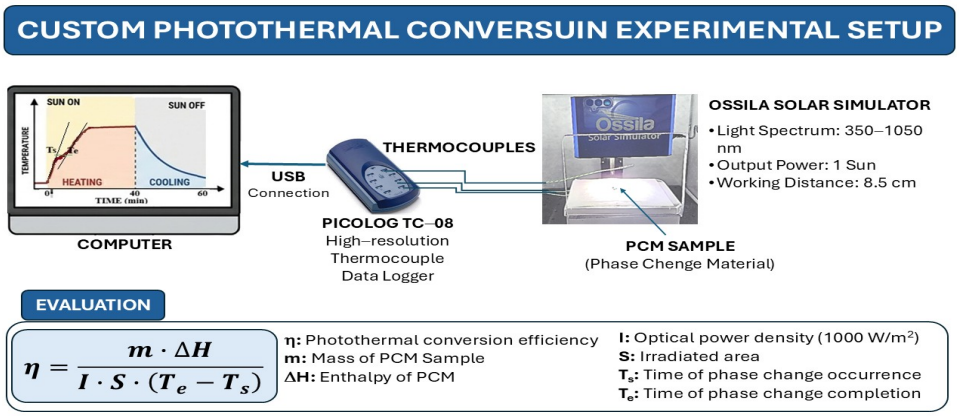


Figure 2. Schematic diagram of the experimental setup for photothermal conversion efficiency evaluation. Source: Gemini (Gemini 3.5 Flash Lite, OpenAI) adapted and modified by the author.

The sample temperature was monitored using a thermocouple connected to a high-resolution PicoLog TC-08 thermocouple data logger (Pico Technology, St Neots, UK) interfaced with a computer. The temperature was continuously recorded during exposure to simulated sunlight and subsequently during the cooling period after the light source

was switched off. After 40 min of irradiation, the simulated sunlight source was turned off, and the sample was allowed to cool naturally to ambient temperature. The photothermal conversion efficiency was calculated according to Equation (2)

$$\eta = \frac{m \cdot \Delta H}{I \cdot S \cdot (T_e - T_s)} \quad (2)$$

where η is the photothermal conversion efficiency, m is the mass of PCM, ΔH is the enthalpy of the PCM, I is the optical power density (1000 W/m^2), S is the irradiated surface area, T_s is the time at the onset of the phase transition, and T_e is the time at the end of the phase transition.

3. Results and Discussion

The investigated PCM is characterized by a high latent heat of phase transition, cyclic stability, and melting at a constant temperature. To investigate the effect of the addition of carbon nanotubes on its thermal properties, DSC measurements were performed. The results of the DSC analysis are presented in Figure 3, while Table 2 summarizes the thermal parameters for each sample, including the onset and end temperatures of the phase transition, the peak transition temperature, and the heat of transition.

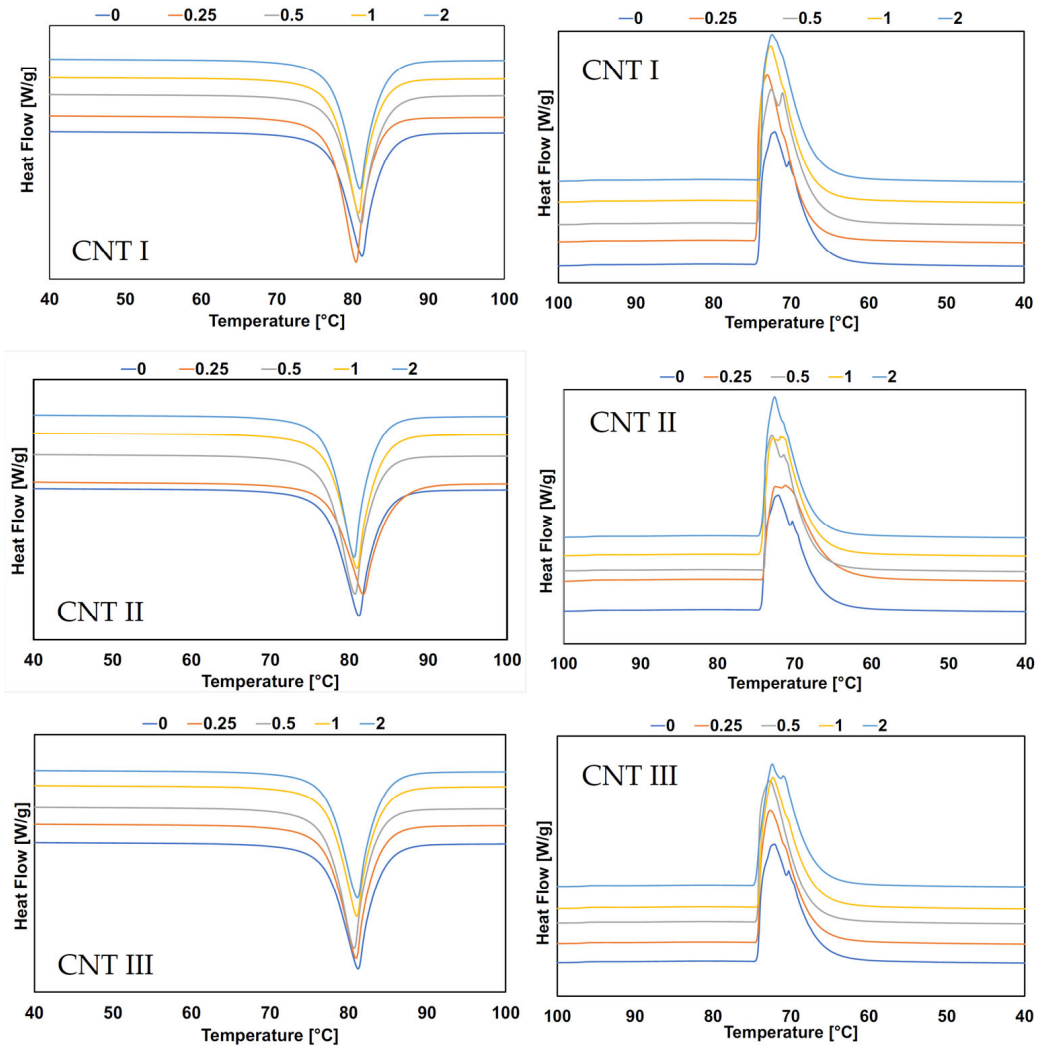


Figure 3. DSC curves of PCM with various carbon nanotube contents for melting (second heating cycle) and crystallization.

Table 2. DSC analysis results of PCM with various carbon nanotube contents during phase transitions.

Samples	$T_{m\ onset}$ [°C]	T_m [°C]	$T_{m\ endset}$ [°C]	Heat of Fusion [J/g]	Theoretical Heat of Fusion [J/g]	$T_{c\ onset}$ [°C]	T_c [°C]	$T_{c\ endset}$ [°C]	Heat of Crystallization [J/g]	ΔT [°C]
PCM_0	74	81	86	215	215	75	72	64	215	9
PCM_025_CNT_I	76	80	84	232	214.5	74	73	67	226	7
PCM_05_CNT_I	75	81	83	220	214.0	74	73	65	223	8
PCM_1_CNT_I	75	81	85	219	213.0	74	73	66	227	8
PCM_2_CNT_I	75	81	85	227	211.0	75	73	66	218	8
PCM_025_CNT_II	77	82	85	220	214.5	74	71	66	212	11
PCM_05_CNT_II	76	81	85	221	214.0	74	73	67	230	8
PCM_1_CNT_II	76	81	86	215	213.0	74	72	66	209	9
PCM_2_CNT_II	76	81	85	230	211.0	75	73	67	219	8
PCM_025_CNT_III	76	81	85	221	214.5	74	73	67	219	8
PCM_05_CNT_III	76	81	84	231	214.0	75	73	67	239	8
PCM_1_CNT_III	76	81	86	220	213.0	74	72	65	206	9
PCM_2_CNT_III	76	81	86	224	211.0	75	72	66	215	9

Large peaks were observed in the DSC curves (Figure 3) at approximately 81 °C and 72 °C during heating and cooling, respectively connected to melting and solidification of PCM. During cooling, the peak was found to consist of several overlapping peaks. This behavior may be attributed to the formation of different crystal structures. Initially, less ordered nucleation sites are formed at approximately 72 °C, followed by the growth of more ordered crystalline structures at a slightly lower temperature of 70 °C. The temperature range over which the phase transition occurs also differs between heating and cooling, amounting to 9 °C and 8 °C, respectively. The widest transition range was observed for the pure PCM, reaching approximately 12 °C during heating and 10 °C during cooling.

The addition of carbon nanotubes slightly affects the phase transition behavior of the investigated material, resulting in slight shifts in the melting and crystallization peak temperatures. For the unmodified PCM_0 sample, the melting temperature was 81 °C, whereas the materials containing CNTs exhibited slightly lower T_m values. The only exception was the PCM_025_CNT_II sample, for which the melting temperature was 82 °C. A slight increase in T_m with increasing nanofiller content was also observed. Despite this minor shift in T_m, it can be concluded that the fundamental thermal characteristics of the PCM are preserved despite the modification. More significant changes were observed in the phase transition temperature range. The onset melting temperature ($T_{m,onset}$) for the CNT-modified samples was generally higher than that of the reference sample (74 °C), reaching values of up to 77 °C, whereas the endset melting temperature ($T_{m,endset}$) shifted toward lower temperatures, reaching 83 °C. This may indicate that the presence of CNTs influences the formation of more defective crystalline structures, whose melting occurs at slightly lower temperatures.

The heat of melting for the initial sample was 215 J/g, whereas for the CNT-containing samples, it was higher across the entire range, varying from 215 J/g for PCM_1_CNT_II to 232 J/g for PCM_0.25_CNT_I. The calculated theoretical heat of fusion values for the respective nanofiller contents were 215 J/g for PCM, 214.5 J/g for PCM_025_CNT, 214 J/g for PCM_05_CNT, 213 J/g for PCM_1_CNT, and 211 J/g for PCM_2_CNT. The higher melting enthalpy observed for the CNT-containing PCM at some CNT concentrations can be related to changes in the crystallization behavior and crystalline microstructure induced by the presence of carbon nanotubes. CNTs can act as heterogeneous nucleation sites, facilitating crystal nucleation during cooling and influencing subsequent crystal growth. This mechanism has been reported for paraffin-based PCMs containing functionalized multi-walled carbon nanotubes, where the well-dispersed nanotubes promoted heterogeneous nucleation and reduced supercooling [23]. Furthermore, a study on paraffin composites

containing ultra-long MWCNTs reported a 6.3% increase in phase-change enthalpy at a CNT loading of 0.5 wt.%, that was attributed to accelerated nucleation and the formation of larger crystallites promoted by the nanotubes [24]. These findings support the hypothesis that, under suitable conditions, CNTs can influence crystallization in a manner that may contribute to an increase in the measured melting enthalpy.

For solidification, the peak maximum temperature for the reference sample was 72 °C, while for the CNT-containing samples, it was slightly higher, reaching 73 °C. The exception was the samples containing nanotubes with an average size of 18–38 nm, for which lower T_c values were observed at CNT contents of 0.25 and 1 wt.%, namely 71 °C and 72 °C, respectively. Changes in the phase transition temperature range were also observed. The onset crystallization temperature ($T_{c,onset}$) for all samples was around 74 °C, whereas the endset temperature ($T_{c,endset}$) for the carbon nanotube-containing samples shifted toward higher temperatures, from 64 °C for the pure PCM to 67 °C. This indicates that the presence of carbon nanotubes causes slight changes in the crystallization temperature, but may also affect the intensity of the process. The crystallization enthalpy showed more pronounced variation, ranging from 206 to 239 J/g, which may indicate both a nucleation effect and complex interactions between the CNTs and the pure PCM.

A change in the degree of supercooling was observed in the PCM samples containing CNTs. For the reference sample, the degree of supercooling was 9 °C, whereas the CNT-modified samples exhibited lower values, with the exception of the sample containing 0.25 wt.% of nanotubes with an average size of 18–38 nm, for which the degree of supercooling was 11 °C. The lower degree of supercooling observed for the PCM samples containing carbon nanotubes suggests that the addition of CNTs facilitates crystallization nucleation, resulting in earlier solidification and a more predictable crystallization process. This is a beneficial effect for thermal energy storage applications, as it improves the reliability of heat release [25].

To further investigate the melting process of the studied samples, the TOPEM® DSC modulated differential scanning calorimetry technique was employed (Figures 4–7). This method enables the total heat flow to be separated into a reversible component, primarily associated with changes in heat capacity and processes occurring under near-equilibrium conditions, and an irreversible component, which includes kinetically controlled processes such as recrystallization, crystal reorganization, and crystal perfection [25–27].

Based on the results obtained from TOPEM® DSC, it was found that the melting transition occurred over a slightly narrower temperature range than in the conventional DSC measurements. The observed shift may be attributed to the lower heating rate used in the modulated measurements. The melting temperature and melting behavior of the materials depend on the heating rate, the amplitude and frequency of modulation, and the characteristic timescale of crystal structure reorganization processes [28,29].

Analysis of the total heat flow curves revealed the presence of a single dominant thermal effect, with its minimum occurring at a temperature of approximately 82 °C. The position of this minimum was approximately independent of the type of CNT and their mass fraction. This result indicates that modification of the material with carbon nanotubes did not cause any significant shift in the temperature of the main melting transition.

In the reversible component of the DSC signal, a broad endothermic effect was recorded over the temperature range of 64–82 °C, with a distinct inflection in the initial temperature range, i.e., approximately 64–73 °C. The broad nature of this effect indicates heterogeneity of the transition and the possible presence of crystals with varying structures and sizes. In organic materials containing a crystalline phase, the effect associated with the melting of crystalline structures that respond to periodic temperature changes over time may involve both surface melting and partial displacement of the crystal–amorphous phase boundary.

This means that the broad signal observed in the 64–82 °C range may indicate the gradual melting of crystalline fractions with different degrees of structural order, rather than a single, ideally homogeneous phase transition [28].

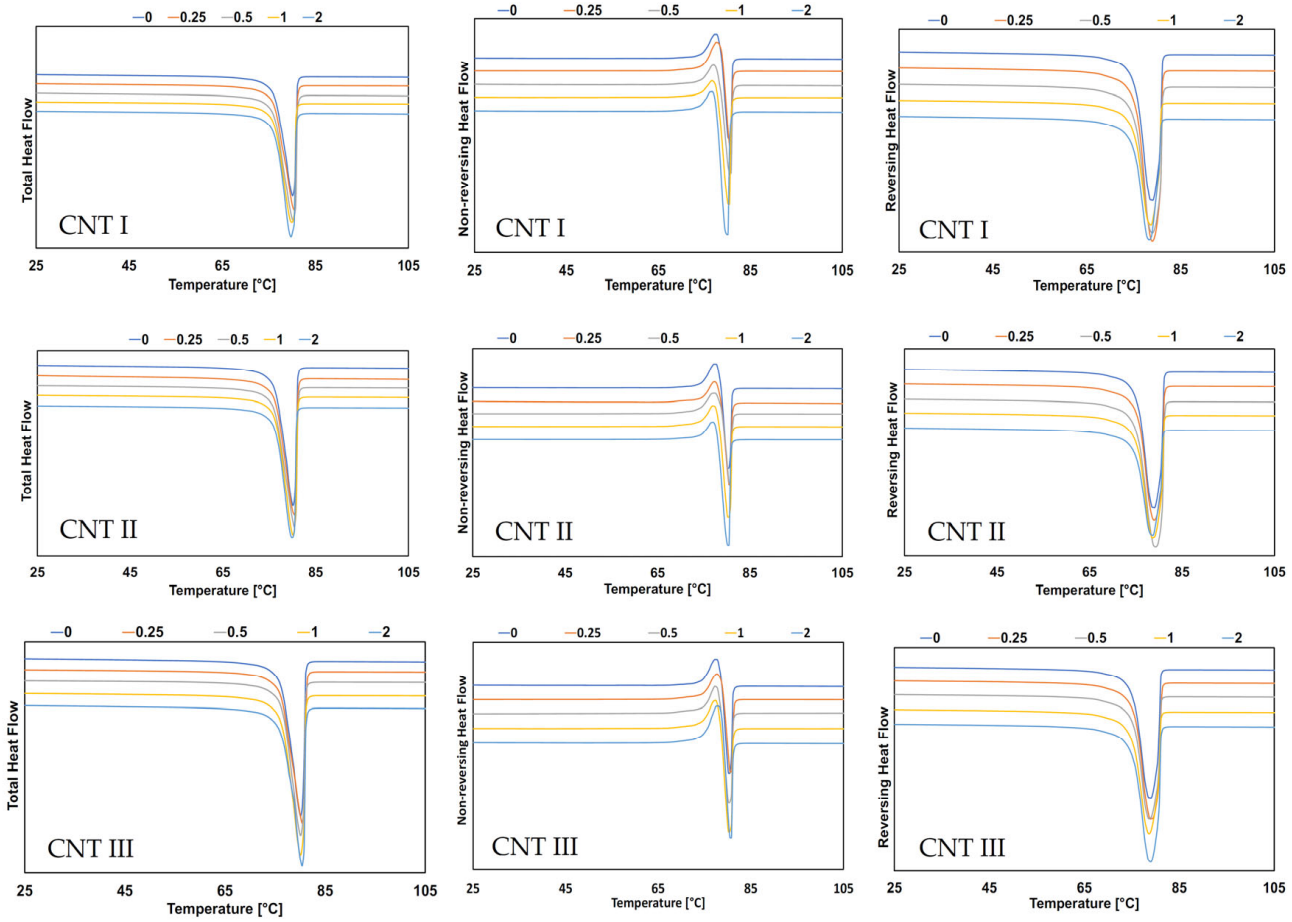


Figure 4. TOPEM DSC curves for total, reversing and non-reversing heat flow of PCM modified with CNT I, II and III.

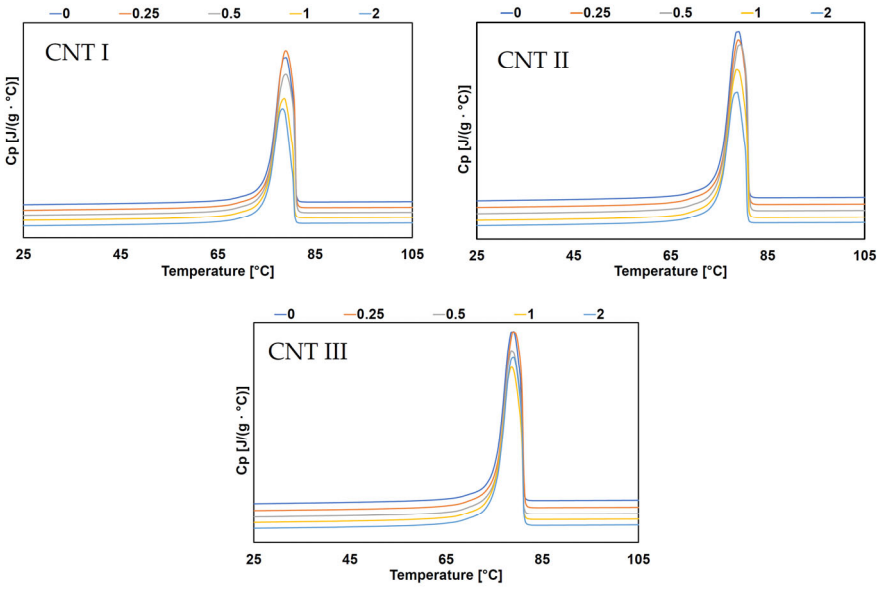


Figure 5. TOPEM DSC heat capacity curves of PCM modified with CNT I, II and III.

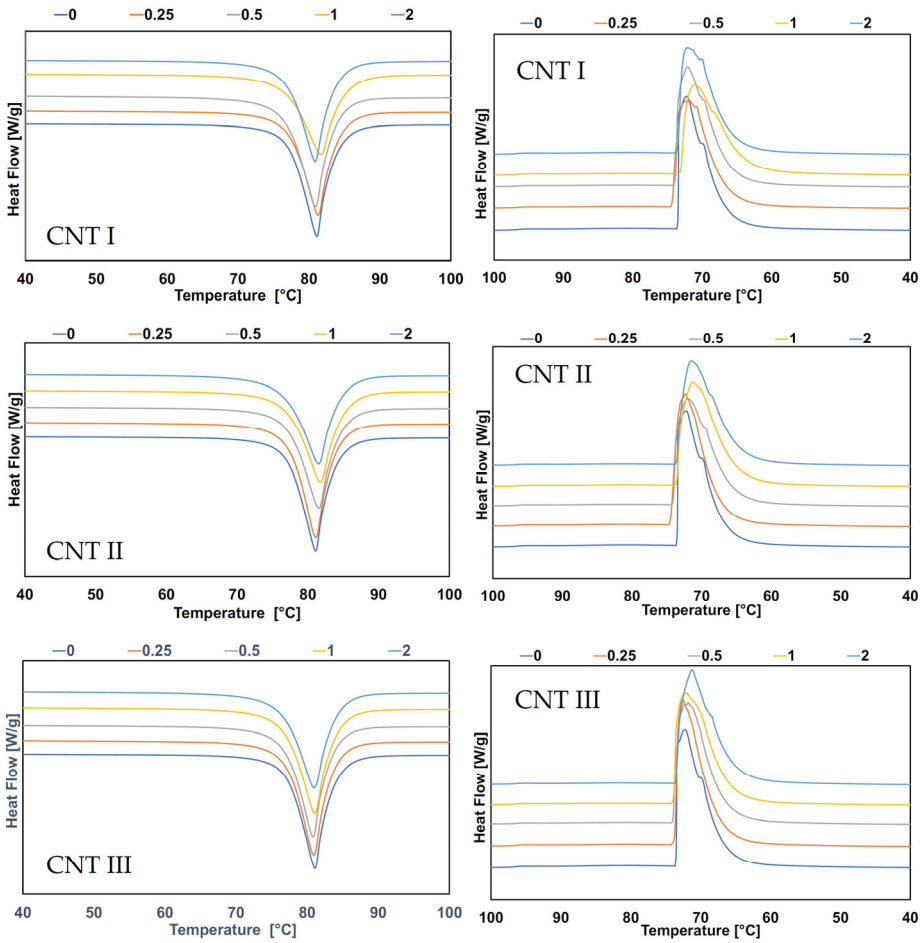


Figure 6. DSC curves of PCM with various CNT contents after 20 melting and solidification cycles in air for melting (**left**) and solidification (**right**).

The most complex behavior was observed in the irreversible component over the temperature range of 64–82 °C. Two overlapping thermal effects were present in this region: the first was exothermic, while the second was endothermic. This behavior can be interpreted as the result of the simultaneous occurrence of reorganization and recrystallization of less stable structures and the melting of more stable crystals.

The first effect, which was exothermic in nature, was relatively broad and exhibited an inflection in the lower temperature range. The width of this effect increased with increasing CNT size, which may indicate more diverse kinetics of crystal structure reorganization processes in the presence of larger nanotubes. In contrast, increasing the nanofiller content resulted in a shortening of this effect by approximately 1 °C. It can be assumed that a higher number of nanotubes increased the available surface area capable of interacting with the crystallizing phase, leading to a more homogeneous process. The temperature of the exothermic peak maximum ranged from 77 to 78 °C, and its position depended on both CNT size and content. As the nanotube size increased, the peak maximum shifted slightly toward higher temperatures, whereas increasing the nanofiller content generally caused a shift toward lower temperatures. This behavior may indicate the competing effects of two factors: restricted mobility of the material segments by larger nanotubes and an increase in the number of active sites for nucleation and crystal reorganization with increasing CNT content. The second effect, which was endothermic in nature, occurred over a narrower temperature range, i.e., 78–83 °C, and depended on both the size and content of the carbon nanotubes. A decrease in CNT size resulted in an increase in the intensity of this effect and a deeper minimum. This result may indicate stronger interactions between the smaller

nanotubes and the crystalline phase, likely associated with their higher specific surface area and greater number of potential interaction sites. Increasing the CNT content, on the other hand, broadened the endothermic effect and shifted the onset of the process by approximately 1 °C toward lower temperatures. Despite these changes, the temperature corresponding to the maximum change in heat flow remained close to 80 °C and showed no clear dependence on either the size or the amount of nanofiller. This indicates that the CNTs primarily modified the temperature range and intensity of the process, while not substantially altering the temperature of the main melting transition.

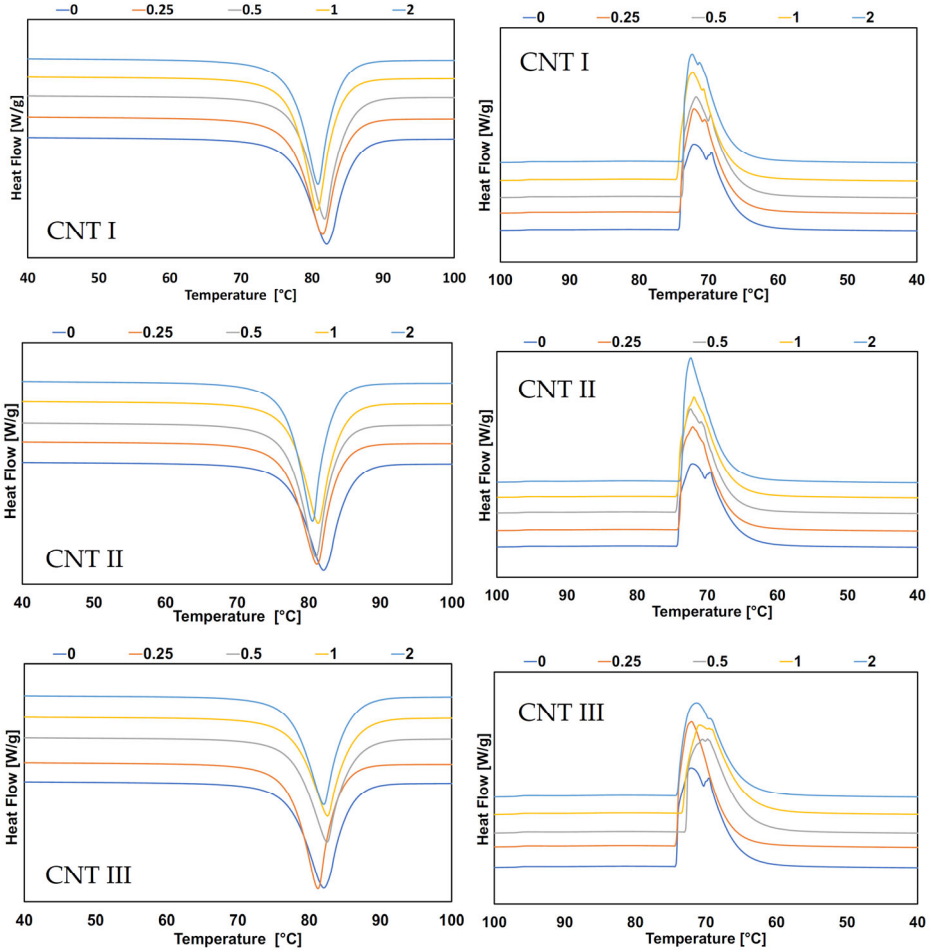


Figure 7. DSC curves of PCM with various CNT contents after 20 melting and solidification cycles in nitrogen for melting (**left**) and solidification (**right**).

Analysis of the dependence of heat capacity on temperature showed that all samples exhibited a broad peak over the temperature range of 65–82 °C, with a maximum at approximately 79 °C. The position of the maximum varied only slightly with changes in nanofiller content. A more pronounced effect of CNTs was observed in terms of the intensity of the change in heat capacity. Its magnitude generally decreased with increasing nanotube content. This may indicate restricted mobility of the material segments and a reduced fraction of structures capable of dynamically responding to temperature modulation. Alternatively, this effect may result from a change in the fraction of the thermally active phase due to the presence of the nanofiller.

The obtained results indicate that CNTs do not substantially alter the operating temperature of the investigated PCM, but rather enable modification of the course of its phase transitions. Therefore, from the perspective of designing materials for thermal energy

storage, it is particularly important to optimize not only the nanotube content but also their size and dispersion.

The results of the DSC analysis after 20 melting and solidification cycles, conducted in air and under a nitrogen atmosphere, are presented in Figures 6 and 7. Tables 3 and 4 summarize the thermal parameters for the individual samples, including the onset and endset temperatures of the phase transition, the peak transition temperature, and the transition enthalpy. Cyclic stability is most commonly assessed based on changes in the phase transition temperature, melting and crystallization enthalpies, and the shape of the DSC curves after a specified number of cycles. The thermal stability of composite PCMs containing carbon-based nanomaterials has been reported in the literature [30–33].

Table 3. Temperatures and heats of phase transitions of PCM with different CNT contents after 20 melting and solidification cycles in air.

Samples	$T_{m\ onset}$ [°C]	T_m [°C]	$T_{m\ endset}$ [°C]	Heat of Fusion [J/g]	$T_{c\ onset}$ [°C]	T_c [°C]	$T_{c\ endset}$ [°C]	Heat of Solidification [J/g]	ΔT [°C]
PCM_0	76	81	86	207	74	72	65	206	9
PCM_025_CNT_I	76	81	86	203	74	72	66	202	9
PCM_05_CNT_I	75	81	85	218	74	72	64	211	9
PCM_1_CNT_I	74	82	87	185	73	71	63	182	11
PCM_2_CNT_I	75	81	85	200	74	72	65	196	9
PCM_025_CNT_II	76	81	86	210	74	72	66	208	9
PCM_05_CNT_II	76	81	86	205	74	72	64	197	9
PCM_1_CNT_II	76	82	86	197	74	71	64	197	11
PCM_2_CNT_II	75	82	86	196	74	72	64	194	10
PCM_025_CNT_III	76	81	85	208	74	73	67	201	8
PCM_05_CNT_III	76	81	85	204	74	72	67	198	9
PCM_1_CNT_III	75	81	85	204	74	72	66	200	9
PCM_2_CNT_III	75	81	85	200	73	71	65	194	10

Table 4. Temperatures and heats of phase transitions of PCM with different CNT contents after 20 melting and solidification cycles in nitrogen.

Samples	$T_{m\ onset}$ [°C]	T_m [°C]	$T_{m\ endset}$ [°C]	Heat of Fusion [J/g]	$T_{c\ onset}$ [°C]	T_c [°C]	$T_{c\ endset}$ [°C]	Heat of Crystallization [J/g]	ΔT [°C]
PCM_0	76	82	87	208	74	72	65	202	10
PCM_025_CNT_I	75	81	86	209	74	72	66	210	9
PCM_05_CNT_I	77	82	86	209	74	72	65	210	10
PCM_1_CNT_I	76	81	85	213	74	72	66	209	8
PCM_2_CNT_I	76	81	85	205	74	72	66	198	8
PCM_025_CNT_II	75	81	85	210	74	72	66	208	9
PCM_05_CNT_II	75	81	85	216	74	72	66	208	9
PCM_1_CNT_II	76	81	86	203	74	72	66	202	9
PCM_2_CNT_II	75	81	84	212	74	72	67	205	8
PCM_025_CNT_III	76	81	85	208	74	72	66	206	9
PCM_05_CNT_III	76	83	88	194	73	70	63	189	13
PCM_1_CNT_III	76	83	87	189	73	71	64	183	12
PCM_2_CNT_III	76	82	86	195	74	71	64	197	11

Analysis of the DSC results obtained after 20 melting and crystallization cycles indicates that repeated thermal cycling did not cause significant degradation of the fundamental phase transition behavior of the investigated PCM, either in the pure material or in the CNT-modified composites. Compared with the initial results, only minor changes in the melting and crystallization temperatures were observed, whereas the transition enthalpy decreased by an average of 8–10%. This result indicates moderate cyclic stability of the material. For the reference PCM sample, after 20 cycles in air, the melting peak temperature

remained practically unchanged at 81 °C, with only a slight shift in the onset and endset temperatures of the transition to 76 °C and 86 °C, respectively. However, the heat stored during melting decreased from approximately 215 J/g to 208 J/g, suggesting a partial loss of the material's latent heat storage capacity.

For the CNT-containing samples, the melting peak temperature also remained essentially unchanged, falling within a similar range of 81–83 °C for measurements conducted both in air and under nitrogen. This indicates that 20 thermal cycles did not cause any substantial shift in the phase transition temperature. As observed for the reference sample, a decrease in the heat of melting relative to the initial samples was observed, particularly pronounced for PCM_1_CNT_I tested in air, for which the lowest value of 185 J/g was recorded, as well as for PCM_05_CNT_III and PCM_1_CNT_III tested under nitrogen, with values of 194 J/g and 189 J/g, respectively. Compared with the melting enthalpies of the initial samples, which ranged from approximately 215 to 232 J/g, the range after 20 cycles was lower and exhibited greater dispersion. This may indicate gradual microstructural reorganization and a partial loss of homogeneity caused by nanotube sedimentation during thermal cycling. A similar trend was observed for crystallization after 20 cycles, with the peak maxima remaining essentially unchanged and falling within the range of 71–73 °C, consistent with the DSC measurements of the initial samples. For the reference PCM sample, the crystallization peak temperature was 72 °C, regardless of the number of cycles or the atmosphere in which they were performed. The changes mainly concerned the transition enthalpy, which decreased from 215 J/g to 206 J/g in air and to 202 J/g under nitrogen. A similar trend was observed for the CNT-modified samples. After 20 crystallization cycles, the enthalpy values ranged from approximately 182 to 211 J/g in air and from 183 to 211 J/g under nitrogen.

In most cases, the transition enthalpy was lower and also more variable compared with the initial samples. The most pronounced decrease was observed for PCM_1_CNT_I in air, where the crystallization enthalpy was 182 J/g, as well as for PCM_1_CNT_III and PCM_05_CNT_III under nitrogen, where the values were 183 J/g and 189 J/g, respectively. The obtained values were also significantly lower than those calculated for the respective CNT mass fractions. This indicates that repeated thermal cycling does not cause a significant shift in the crystallization temperatures but does affect the intensity of the process. In practical terms, this suggests a partial modification of the crystal structure or the degree of structural ordering of the material, resulting in a lower effective transition enthalpy. After 20 cycles, a noticeable change in the degree of supercooling was also observed. For the reference sample, the value increased from 9 °C to 9–10 °C, depending on the atmosphere. This may suggest that cyclic testing affects the nucleation kinetics. For most of the CNT-modified samples, the degree of supercooling was comparable to or lower than that of the reference sample. The exceptions were PCM_1_CNT_II, PCM_05_CNT_III, and PCM_1_CNT_III, for which an increase to 11–13 °C was observed, with higher values obtained for cycles performed under a nitrogen atmosphere.

The results obtained for the PCM are comparable with literature data for PCMs modified with carbon nanotubes, where a decrease in transition enthalpy has also been reported, although the change in enthalpy was considerably smaller [30]. This may indicate that the system used in the present study is more sensitive to repeated phase transitions, or that CNTs affect the organization of the crystalline phase in a manner dependent on their size and mass fraction. Other studies have shown that the effect of CNTs on transition enthalpy is not always unambiguous. On the one hand, CNTs improve thermal conductivity; on the other hand, a reduction in the mass fraction of the PCM phase decreases the enthalpy referred to the total mass of the composite. This phenomenon may partially explain the reduction in the melting and crystallization enthalpies observed in the investigated samples [31,33].

The results reported by Sarı et al. [32] are consistent with the observations obtained for the PCM, for which the melting and crystallization peak temperatures remained stable after 20 cycles. At the same time, the results of the present study indicate that the stability of the phase transition temperatures does not necessarily imply the complete preservation of energy storage capacity, as the transition enthalpies underwent more pronounced changes. The literature has shown that the effect of carbon nanotubes on cyclic stability depends on their dispersion, length, diameter, surface functionalization, and compatibility with the PCM. The stability of nanoparticles in both the liquid and solid phases of the PCM is one of the key factors determining the reproducibility of the composite's thermal properties. In the investigated samples, possible CNT agglomeration or partial migration during successive cycles may have limited their effectiveness as nucleation sites and contributed to the reduction in crystallization enthalpy [34].

The results of the thermogravimetric analysis of the CNT-modified PCM are presented in Figure 8 as TG and DTG curves. Table 5 summarizes the temperatures corresponding to successive mass losses ($T_{1\%}$, $T_{5\%}$, $T_{10\%}$, $T_{50\%}$), the temperature of the maximum mass loss rate (T_{DTGmax}), and the amount of solid residue remaining at 600 °C. These parameters enable the assessment of the material's resistance to thermal decomposition and the determination of the effect of the type and content of carbon nanotubes on the degradation behavior.

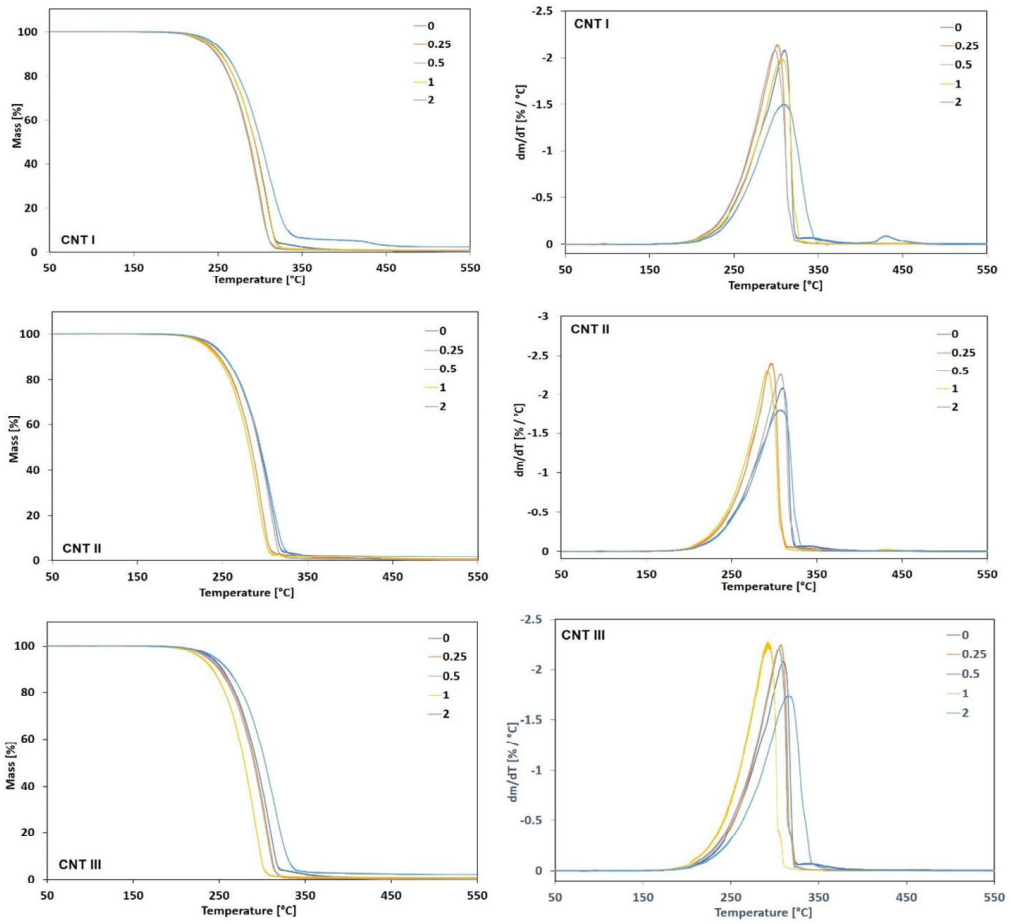


Figure 8. TG and DTG curves of PCM with different CNT contents.

Table 5. Thermal stability of PCM with different CNT contents.

Samples.	IPDT [°C]	$T_{1\%}$ [°C]	$T_{1\%}$ * [°C]	$T_{5\%}$ [°C]	$T_{5\%}$ * [°C]	$T_{10\%}$ [°C]	$T_{10\%}$ * [°C]	$T_{50\%}$ [°C]	$T_{50\%}$ * [°C]	$T_{max\ DTG}$ [°C]	Residue at 600 °C [%]	Residue at 600 °C * [%]
PCM_0	291	213	212	240	240	253	253	294	294	310	0.03	0.03
PCM_025_CNT_I	288	209	208	235	234	248	248	288	288	302	0.38	0.13
PCM_05_CNT_I	289	209	208	234	234	248	247	287	286	299	0.56	0.06
PCM_1_CNT_I	299	212	211	239	238	253	252	293	293	307	0.87	0
PCM_2_CNT_I	328	218	216	245	244	259	258	301	300	309	2.28	0.28
PCM_025_CNT_II	282	209	208	234	233	247	247	284	284	297	0.10	0
PCM_05_CNT_II	293	213	212	239	239	253	253	293	293	308	0.46	0
PCM_1_CNT_II	288	206	204	231	230	244	244	281	281	292	0.83	0
PCM_2_CNT_II	314	212	211	239	238	253	252	295	294	305	1.91	0
PCM_025_CNT_III	289	210	209	236	236	250	250	291	292	307	0.24	0
PCM_05_CNT_III	292	209	208	235	235	249	249	290	290	305	0.59	0.09
PCM_1_CNT_III	287	203	202	228	228	242	241	279	279	293	0.91	0
PCM_2_CNT_III	327	215	214	244	244	259	259	303	303	316	2.22	0.22

* Values normalized to the PCM mass in the nanocomposite.

Analysis of the TG curves showed that the investigated samples exhibited essentially a single-step thermal decomposition, primarily associated with the degradation of the organic PCM phase. For the reference PCM sample, the temperature corresponding to a 50% mass loss was 294 °C, while the temperature of the maximum degradation rate, determined from the DTG curve, was 310 °C. The residue after heating to 600 °C was negligible, amounting to 0.03%. The incorporation of CNTs modified the thermal decomposition behavior. However, the effect of the nanotubes was not entirely unambiguous and depended on both their mass content and size. The most pronounced trend was observed for the temperatures corresponding to the initial stages of degradation, $T_{1\%}$, $T_{5\%}$, and $T_{10\%}$. Within the individual CNT groups, increasing their content generally shifted these temperatures toward higher values. This indicates that increasing the CNT fraction reduced the susceptibility of the material to initial thermal decomposition. For nanotubes with an outer diameter of 7–16 nm, the $T_{1\%}$ temperature increased from 209 °C for PCM_025_CNT_I to 218 °C for PCM_2_CNT_I. For CNT_II, the $T_{1\%}$ values increased from 206 °C to 213 °C, whereas for CNT_III, the values increased from 203 °C to 215 °C. A similar trend was observed for $T_{50\%}$. Compared with the reference sample, for which $T_{50\%}$ is 294 °C, this parameter increased to 301 °C for PCM_2_CNT_I, 295 °C for PCM_2_CNT_II, and 303 °C for PCM_2_CNT_III. The obtained results indicate that the highest CNT content, amounting to 2 wt.%, had a beneficial effect on the material's resistance to the main stage of thermal degradation. This effect was particularly pronounced for nanotubes CNT_I and CNT_III. An increase in $T_{50\%}$ indicates that a larger fraction of the material remained stable up to a higher temperature before undergoing substantial decomposition.

The temperature of the maximum mass loss rate, T_{DTGmax}, for the reference PCM_0 sample was 310 °C. The incorporation of CNTs resulted in varying changes in this parameter. For nanotubes with a size of 7–16 nm, the T_{DTGmax} values ranged from 299 to 309 °C; for CNTs with a size of 18–38 nm, they ranged from 292 to 308 °C; whereas for the largest nanotubes, with a size of 48–78 nm, the values ranged from 293 to 316 °C. The highest maximum degradation rate temperature, 316 °C, was recorded for the PCM_2_CNT_III sample. This value was 6 °C higher than that of the reference sample. This result indicates that the largest CNTs at the highest mass fraction produced the most pronounced shift in the main decomposition stage toward higher temperatures.

For samples containing smaller and medium-sized nanotubes, this effect was less pronounced, and in some cases, a decrease in T_{DTGmax} was even observed. The absence of a clear relationship between T_{DTGmax} and CNT size may result from the competing effects of several factors, such as the degree of nanotube dispersion, their tendency to agglomerate,

the contact area with the organic phase, and limitations in the transport of decomposition products. Therefore, CNT content alone is insufficient to predict the thermal stability of the composite.

Additionally, the integral procedural decomposition temperature (IPDT) was determined [35,36], and the mass loss and residue values at 600 °C were recalculated by subtracting the contribution of the solid fraction introduced by the CNT additive. The results are presented in Table 4. Calculations show that the IPDT increased by 13%, 9%, and 12% only for samples containing 2 wt.% of CNT_I, CNT_II, and CNT_III, respectively. A slight increase (from 1% to 2%) was also observed for the 1 wt.% addition. For the remaining samples, the changes were insignificant, suggesting that the dilution effect does not significantly influence thermal stability. Previous studies have indicated that such effects are typically observed at additive loadings of 10 wt.% or higher. Furthermore, the recalculated characteristic temperatures, adjusted to account for the mass of the added nanofillers, differed only slightly from the originally measured values. Temperature shifts of 1–2 °C were observed; however, the number of samples exhibiting such differences decreased with increasing mass loss. In particular, a shift in T_{50}% was observed in only a few samples. Nevertheless, the overall trends remained consistent across the entire measurement range.

The residue for the reference sample after heating to 600 °C is very low, at approximately 0.03%. In samples containing carbon nanotubes (CNTs), the residue corresponds to the remaining carbonaceous phase. The highest residue value was observed for PCM_2_CNT_I (2.28%, which equates to 0.28% after subtracting the mass of the nanotubes themselves), while for PCM_2_CNT_III, the value was 2.22% (0.22%). Other values recorded were 0.13% for PCM_025_CNT_I, 0.06% for PCM_05_CNT_I, and 0.09% for PCM_05_CNT_III. Interestingly, for the remaining materials, the residue was 0. Across all groups, a general trend toward increasing residue content with increasing CNT content was observed. However, this relationship was not perfectly linear, which may result from differences in nanotube dispersion and the crystallinity of the individual samples. The highest residue content was obtained for the smallest nanotubes, whereas the lowest was observed for the intermediate-sized CNTs. These differences may be related to variations in specific surface area and the degree of nanofiller agglomeration. The improvement in thermal stability following the incorporation of CNTs can be explained by several overlapping mechanisms. First, nanotubes may form a three-dimensional network within the matrix that restricts the mobility of organic chains or components. Second, CNTs may act as a barrier hindering the transport of volatile degradation products and limiting their release from the material. Third, the thermally stable carbonaceous phase may promote the formation of a protective residue that partially inhibits further material decomposition. Similar mechanisms have been described in the literature for paraffin-based composites containing CNTs. Studies of paraffin/CNT systems have reported a shift in the maximum degradation temperature toward higher values, which was interpreted as an improvement in the thermal resistance of paraffin due to the presence of nanotubes. In one such system, the addition of CNTs increased the maximum degradation rate temperature from 209.4 °C for pure paraffin to 218.0 °C [37].

A similar effect was also observed in composites in which paraffin was immobilized within a porous matrix containing CNTs. It was demonstrated that the presence of a three-dimensional CNT framework improved the thermal stability of paraffin and limited its migration during heating. In the case of microencapsulated PCMs with a SnO_2/CNT shell, the retardation of paraffin degradation was attributed to the protective effect of the shell, which limited direct contact between the organic phase and the surrounding environment [38,39].

The results obtained for the PCM are therefore consistent with literature reports indicating that CNTs can improve the thermal stability of organic PCMs. However, it should be emphasized that this effect depends on the concentration and morphology of the nanotubes. In the investigated system, the greatest improvement in thermal stability, assessed based on the shifts in $T_{1\%}$, $T_{50\%}$, and T_{DTGmax}, was observed primarily for samples containing 2 wt.% CNTs. At the same time, a decrease in the maximum degradation rate temperature was observed for some samples with lower nanofiller contents, which may be attributed to more efficient heat transfer in the CNT-modified systems.

The results of the FTIR analysis are presented in Figure 9.

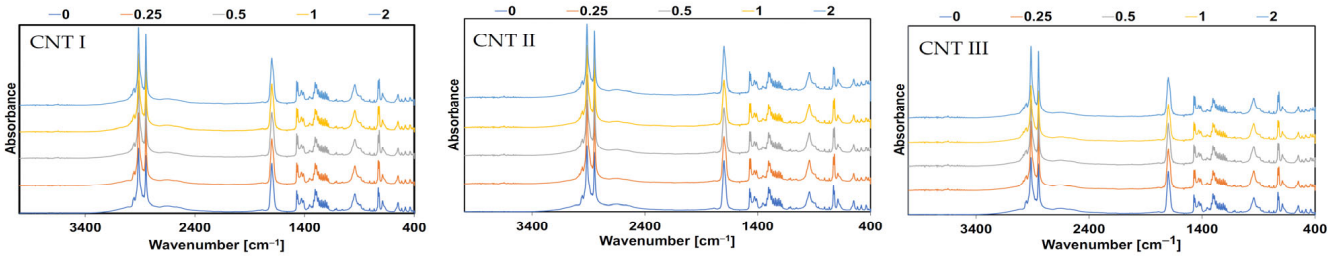


Figure 9. FTIR spectra for PCM without and modified with different CNT additions.

Analysis of the attenuated total reflectance Fourier-transform infrared (ATR-FTIR) spectrum of the PCM sample revealed the presence of bands characteristic of long-chain aliphatic compounds containing carboxyl groups. The recorded bands indicate the presence of hydroxyl and carbonyl groups, as well as methylene group vibrations forming a long hydrocarbon chain. The spectrum is typical of an organic phase change material with an ordered solid-state structure. In the broad range of 3300–2500 cm^{-1}, stretching vibrations of the O–H group associated with the carboxyl group are observed. Such a broad band is characteristic of carboxyl groups, which form hydrogen-bonded dimers in the condensed phase. The presence of this band confirms the contribution of acidic groups or other strongly hydrogen-bonded hydroxyl groups to the structure of the investigated material [40]. The subsequent bands, located at approximately 2954 cm^{-1}, 2914 cm^{-1}, and 2847 cm^{-1}, are associated with the stretching vibrations of aliphatic groups. The band at 2954 cm^{-1} can be attributed to the asymmetric stretching vibrations of the methyl (CH_3) groups. The strong band at 2914 cm^{-1} corresponds to the asymmetric stretching vibrations of the methylene (CH_2) groups, whereas the signal at 2847 cm^{-1} is associated with the symmetric stretching vibrations of the CH_2 groups. This band is characteristic of the symmetric stretching vibrations of aliphatic methylene groups [40–43]. In the range of 1750–1600 cm^{-1}, a band associated with the vibrations of the carbonyl group and possible double bonds is observed. The very intense signal near 1700 cm^{-1} corresponds to the stretching vibrations of the C=O bonds in the carboxyl group. The position of this band is consistent with the presence of undissociated –COOH groups. For lipid materials and long-chain organic compounds, the bands at approximately 2920 cm^{-1}, 2850 cm^{-1}, and 1700–1740 cm^{-1} are characteristic signals of CH_2 and C=O groups, respectively [40,42]. The signal at approximately 1472 cm^{-1} corresponds to the scissoring deformation vibrations of CH_2 groups. The subsequent broad range of 1400–1150 cm^{-1} contains numerous maxima at approximately 1354 cm^{-1}, 1303 cm^{-1}, 1291 cm^{-1}, 1275 cm^{-1}, 1259 cm^{-1}, 1243 cm^{-1}, 1228 cm^{-1}, 1213 cm^{-1}, 1198 cm^{-1}, 1184 cm^{-1}, and 1110 cm^{-1}. These bands can be attributed primarily to rocking, twisting, and deformation vibrations of CH_2 groups along the long aliphatic chain. Stretching vibrations of the C–O bonds of the carboxyl group may also occur in this region [44–46]. The characteristic "comb-like" shape of this part of the spectrum may result from mechanical coupling between the vibrations of successive CH_2 groups in an ordered aliphatic chain. This phenomenon

has also been reported for long-chain fatty acids, including stearic acid [44,45]. The signal near 924 cm^{-1} may be associated with the deformation vibrations of the O–H group and with vibrations of carboxyl groups involved in the formation of hydrogen-bonded dimers. The presence of CNTs did not result in the appearance of any clearly identifiable new bands in the ATR-FTIR spectrum. This may be attributed to the low mass fraction of the nanotubes, their relatively weak infrared activity, and the overlap of CNT signals with the intense bands of the organic matrix. The absence of new bands suggests that no new, readily detectable functional groups were formed during composite preparation. At the same time, changes in the intensity, width, or position of selected bands may indicate physical interactions between the CNTs and PCM, such as restricted chain mobility, changes in crystal packing, or modification of the degree of ordering of the organic phase.

SEM analysis of the CNT-modified PCM (Figure 10) confirmed a good and relatively homogeneous dispersion of CNTs throughout the PCM matrix. No pronounced CNT agglomeration or large CNT clusters were observed, indicating that the modification procedure enabled an effective dispersion and incorporation of the carbon nanotubes into the PCM matrix.

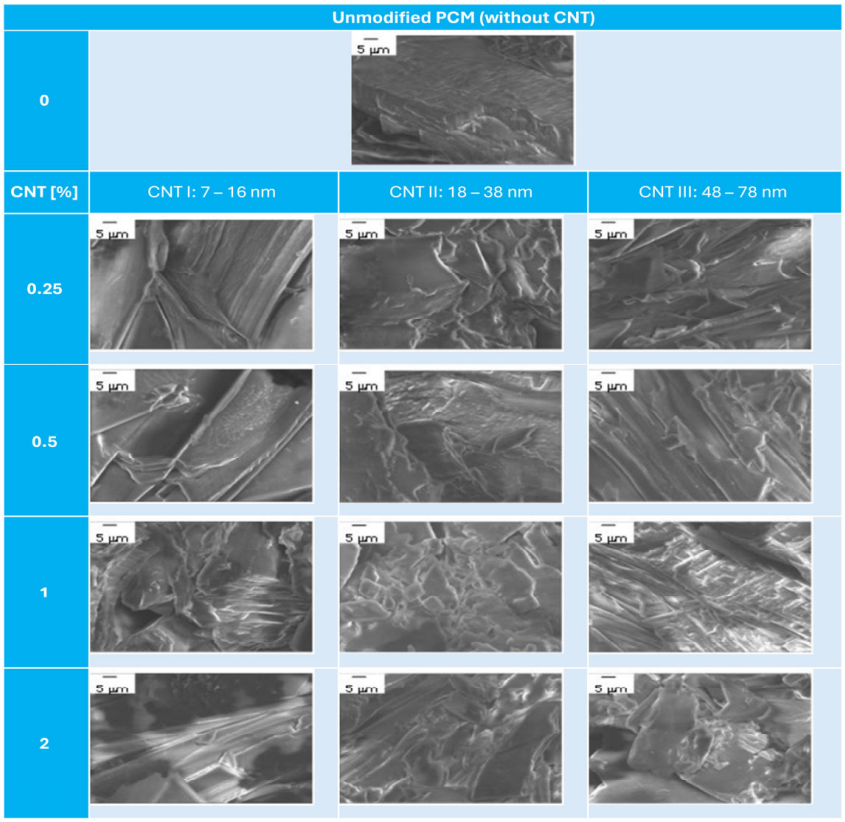


Figure 10. SEM microphotographs of PCM with different CNT contents (×5000).

The microscopic observations also revealed a well-developed crystalline morphology of the PCM matrix. This highly ordered structure is consistent with the characteristic behavior of fatty acid-based PCMs, which tend to form well-defined crystalline structures upon solidification. The presence of a well-developed crystalline phase may also contribute to the thermal storage behavior of the PCM, as the formation and disruption of this ordered structure are associated with the phase transition responsible for latent heat storage. Moreover, the incorporation of a low amount of CNTs did not result in any clearly visible disruption of the overall crystalline morphology of the PCM matrix. Figure 11 presents the results of the

photothermal conversion tests of the PCM/CNT composites containing carbon nanotubes of different sizes and mass fractions.

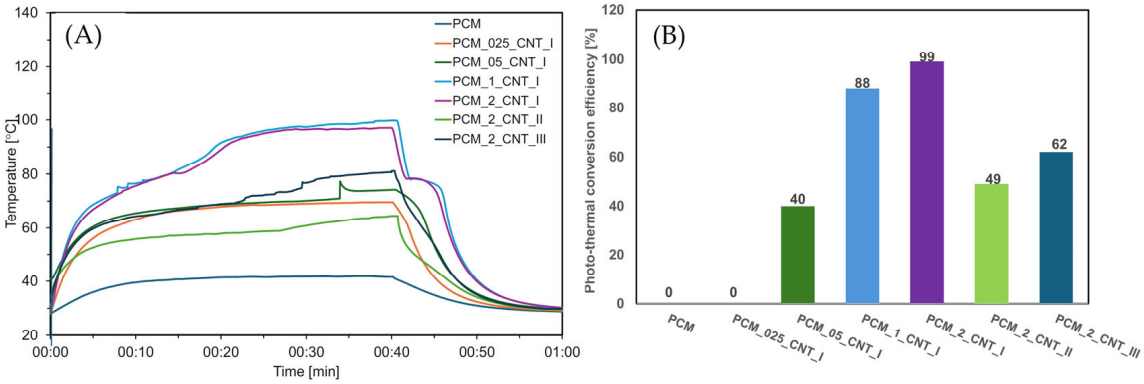


Figure 11. (**A**) Temperature evolution curves of composites during solar–thermal conversion test, (**B**) calculated photothermal conversion efficiency.

The study was conducted using a solar radiation simulator, with temperature changes in the samples analyzed during irradiation and after the radiation source was switched off. The incorporation of CNTs was intended to increase radiation absorption and improve the rate of conversion of light energy into heat. Carbon nanotubes are capable of efficiently absorbing radiation over a broad spectral range and subsequently transferring the absorbed energy in the form of heat to the PCM [47,48]. The reference PCM sample did not exhibit a pronounced effect associated with a phase transition during irradiation. Initially, a relatively slow increase in temperature was observed, followed by the temperature reaching approximately 40 °C after about 10 min and remaining practically unchanged until the end of irradiation. After the lamp was switched off, the temperature decreased approximately linearly and reached the ambient temperature after another 10 min. This behavior indicates the limited ability of the unmodified PCM to directly absorb radiation and convert light energy into heat, which is typical of conventional organic PCMs [47,48]. The addition of CNTs increased the temperature reached during irradiation and accelerated the rate of temperature increase. The heating rate increased with increasing nanotube content, indicating their active contribution to radiation absorption and photothermal conversion. A similar effect has been reported for other PCM composites containing CNTs, in which the nanotubes act as radiation absorbers and thermally conductive elements within the composite network [47,48]. For the PCM_025_CNT_I sample, no distinct inflection of the temperature curve that could be unequivocally attributed to a phase transition was observed either. After approximately 10 min of irradiation, the sample temperature increased to approximately 65 °C and then remained at a similar level until the end of the experiment. After the lamp was switched off, however, an inflection appeared in the initial stage of the cooling curve. This may indicate the superposition of sensible heat release and the onset of crystallization. During crystallization, part of the energy is released as latent heat, which may temporarily slow the decrease in temperature. At a CNT content of 0.5 wt.% and above, a significantly faster increase in temperature was observed. After approximately 3 min of irradiation, the samples reached temperatures exceeding 60 °C. This result confirms that increasing the CNT content improves the material's ability to absorb radiation and accelerates heat transport throughout the composite. At the same time, the heating rate depends not only on the nanotube content itself but also on their size, degree of dispersion, and the manner in which they form a conductive network within the matrix. For the PCM_05_CNT_I sample, the phase transition became apparent only after a longer irradiation period. After approximately 33 min, a rapid increase in temperature was observed, followed by a decrease. This

behavior may be associated with a non-uniform CNT distribution and the local formation of regions with enhanced radiation absorption. After the solar simulator was switched off, the temperature decrease in the PCM_05_CNT_I sample was not linear. A similar behavior was observed for the PCM_025_CNT_I sample. The deviation from linear cooling may indicate the release of latent heat during crystallization. The greatest temperature increase was observed for the samples containing 1 and 2 wt.% thinnest and longest CNTs (CNT_I). The PCM_1_CNT_I and PCM_2_CNT_I samples reached a temperature of approximately 100 °C, and the phase transition began earliest in these samples. After the lamp was switched off, the temperature initially decreased rapidly; after approximately 2 min, a slowdown in the cooling process was observed, lasting for about 3 min, after which the temperature began to decrease more rapidly again. The change in the slope of the cooling curve may be associated with PCM crystallization and the release of latent heat. The most pronounced effect observed for the smallest CNTs may result from their higher specific surface area, greater ability to form a homogeneous conductive network, and larger number of contact sites with the organic phase. The results obtained using the solar simulator are reflected in the photothermal conversion efficiencies presented in Figure 11B. The effect of nanotube size was not unambiguous; however, the highest efficiency was obtained for the thinnest and longest CNTs. Within this group, the photothermal conversion efficiency increased with increasing nanofiller content: it was 40% for PCM_05_CNT_I, whereas for the samples containing 1 and 2 wt.% CNTs, it reached 88% and 99%, respectively. A higher number of nanotubes increases the probability of radiation absorption, while their dimensions promote more homogeneous dispersion and a larger contact area with the matrix. As a result, radiation energy can be absorbed more effectively and transferred to the PCM. For CNTs II and III, the photothermal conversion efficiency was lower, and amounted to only 49% and 62%, respectively. This indicates that simply increasing the CNT content does not guarantee maximum photothermal conversion efficiency. Larger nanotubes may have a greater tendency to agglomerate; consequently, some of the energy may be absorbed locally but not efficiently transferred throughout the entire material volume. The obtained results are consistent with literature reports on CNT-containing composite PCMs, which have demonstrated that the presence of nanotubes can enable rapid heating of the material to approximately 100 °C and achieve high photothermal conversion efficiency while maintaining latent heat storage capacity. In other composites containing CNTs and paraffin or fatty acids, high efficiency was achieved through the combination of strong radiation absorption by the carbonaceous phase and enhanced thermal conductivity [47,49]. The literature also emphasizes that the highest photothermal conversion efficiencies are achieved in composites in which CNTs form a three-dimensional or hierarchical conductive network. Such a structure increases the number of heat-transfer pathways, reduces interfacial thermal resistance, and facilitates uniform energy distribution throughout the material. For comparison, photothermal conversion efficiencies exceeding 90% have been reported for systems containing porous carbon matrices and CNTs, confirming the importance not only of the type of nanofiller but also of its spatial organization [48,50,51].

4. Conclusions

In this study, the effect of functionalized CNT characteristics on the key functional properties of organic phase change materials was systematically investigated. PCM/CNT composites containing CNTs with different characteristics were prepared and studied. The results revealed that the incorporation of carbon nanotubes had only a minor effect on the phase change behavior of the PCM/CNT systems, resulting in slight shifts in the melting and crystallization peak temperatures. In contrast, the phase change enthalpy values obtained from DSC measurements were significantly higher for the CNT-modified PCMs, which may

indicate that the presence of CNTs provided additional nucleation sites for crystallization and thus promoted the crystallization process. Analysis of the DSC results obtained after 20 melting–solidification cycles shows a decrease in melting enthalpy, which indicates a change in the thermal energy storage capacity during cycling, and further investigation would be required to assess the long-term cycling stability of the studied materials. TG analysis showed that the highest CNT content investigated, i.e., 2 wt.%, had a beneficial effect on the material's thermal stability, particularly during the main stage of thermal degradation. FTIR analysis confirmed the absence of new absorption bands, suggesting that no new functional groups were formed during composite preparation. Photothermal conversion studies revealed the highest conversion efficiency for composites containing the thinnest and longest CNTs (CNT_I). For a CNT concentration of 2 wt.%, the photothermal conversion efficiency reached approximately 98%. In comparison, composites containing CNT_II and CNT_III exhibited substantially lower photothermal conversion efficiencies, of approximately 50%. These results demonstrate that simply increasing the CNT content does not necessarily ensure maximum photothermal conversion efficiency and highlight the importance of CNT size in determining the photothermal performance of the composites. Overall, the results confirm that the appropriate selection of CNT size and concentration can improve the functional performance of organic PCMs while preserving their phase transition characteristics and thermal cycling stability.

Author Contributions: Conceptualization, B.M. and K.P.; methodology, B.M. and K.P.; formal analysis, B.M. and K.P.; investigation, B.M., A.P., J.P. and M.S., data curation, B.M. and J.P.; writing—original draft preparation, B.M., A.P. and K.P.; writing—review and editing, B.M. and K.P.; visualization, B.M. and J.P.; supervision, K.P.; project administration, K.P.; funding acquisition, K.P. All authors have read and agreed to the published version of the manuscript.

Funding: The authors are grateful to the National Center for Research and Development for financial support under Contract No. NTE2/0004/2022 2022 with the acronym MMC. The studies were financed by the "Excellence Initiative—Research University" program (IDUB) at AGH University of Krakow and by a subsidy of the Minister of Science and Higher Education for the AGH University of Kraków.

Institutional Review Board Statement: Not applicable.

Informed Consent Statement: Not applicable.

Data Availability Statement: The original contributions presented in this study are included in the article. Further inquiries can be directed to the corresponding author.

Conflicts of Interest: The author Martyna Sioła is an employee of MDPI; however, she does not work for the journal Applied Sciences at the time of submission and publication.

References

1. Sharma, A.; Tyagi, V.V.; Chen, C.R.; Buddhi, D. Review on thermal energy storage with phase change materials and applications. *Renew. Sustain. Energy Rev.* **2009**, *13*, 318–345. [CrossRef]
2. Macherzyńska, B.; Pitera, A.; Nowicka-Dunal, K.; Pielichowska, K. Polyethylene-Based Phase Change Materials Modified with Hexagonal Boron Nitride Nanoparticles with Enhanced Thermal Stability and Thermal Conductivity. *Materials* **2026**, *19*, 455. [CrossRef]
3. Pielichowska, K.; Pielichowski, K. Phase change materials for thermal energy storage. *Prog. Mater. Sci.* **2014**, *65*, 67–123. [CrossRef]
4. Jouhara, H.; Żabnieńska-Góra, A.; Khordehgah, N.; Ahmad, D.; Lipinski, T. Latent thermal energy storage technologies and applications: A review. *Int. J. Thermofluids* **2020**, *5–6*, 100039. [CrossRef]
5. Nazir, H.; Batool, M.; Bolivar Osorio, F.J.; Isaza-Ruiz, M.; Xu, X.; Vignarooban, K.; Phelan, P.; Inamuddin; Kannan, A.M. Recent developments in phase change materials for energy storage applications: A review. *Int. J. Heat Mass Transf.* **2019**, *129*, 491–523. [CrossRef]

6. Mao, S.; Liu, Y.; Wu, X.; Zhang, L.; Chen, J.; Zhou, T. Thermal energy storage performance, application and challenge of phase change materials: A review. *Energy Storage Sav.* **2025**, *4*, 300–322. [CrossRef]
7. Abhat, A. Low temperature latent heat thermal energy storage: Heat storage materials. *Sol. Energy* **1983**, *30*, 313–332. [CrossRef]
8. Sharma, R.K.; Ganesan, P.; Tyagi, V.V.; Metselaar, H.S.C.; Sandaran, S.C. Developments in organic solid-liquid phase change materials and their applications in thermal energy storage. *Energy Convers. Manag.* **2015**, *95*, 193–228. [CrossRef]
9. Zhou, D.; Zhao, C.Y.; Tian, Y. Review on thermal energy storage with phase change materials (PCMs) in building applications. *Appl. Energy* **2012**, *92*, 593–605. [CrossRef]
10. Yuan, Y.; Zhang, N.; Tao, W.; Cao, X.; He, Y. Fatty acids as phase change materials: A review. *Renew. Sustain. Energy Rev.* **2014**, *29*, 482–498. [CrossRef]
11. Pielichowski, K.; Flejtuch, K. Differential Scanning Calorimetry Study of Blends of Poly(ethylene glycol) with Selected Fatty Acids. *Macromol. Mater. Eng.* **2003**, *288*, 259–264. [CrossRef]
12. Wang, Z.; Huang, G.; Jia, Z.; Gao, Q.; Li, Y.; Gu, Z. Eutectic Fatty Acids Phase Change Materials Improved with Expanded Graphite. *Materials* **2022**, *15*, 6856. [CrossRef]
13. Al-Ahmed, A.; Sarı, A.; Mazumder, M.A.J.; Salhi, B.; Hekimoğlu, G.; Al-Sulaiman, F.A.; Inamuddin. Thermal energy storage and thermal conductivity properties of fatty acid/fatty acid-grafted-CNTs and fatty acid/CNTs as novel composite phase change materials. *Sci. Rep.* **2020**, *10*, 15388. [CrossRef]
14. Wu, W.Y.; Da Yeo, G.M.; Wang, S.; Liu, Z.; Loh, X.J.; Zhu, Q. Recent Progress in Polyethylene-enhanced Organic Phase Change Composite Materials for Energy Management. *Chem. Asian J.* **2023**, *18*, e202300391. [CrossRef]
15. Yu, D.; Qiu, Y.; Zhang, X. Role of nano-copper in discharging performance of latent heat storage unit. *Int. Commun. Heat Mass Transf.* **2023**, *144*, 106748. [CrossRef]
16. Kibria, M.A.; Anisur, M.R.; Mahfuz, M.H.; Saidur, R.; Metselaar, I.H.S.C. A review on thermophysical properties of nanoparticle dispersed phase change materials. *Energy Convers. Manag.* **2015**, *95*, 69–89. [CrossRef]
17. Ulker, N.; Bulut, H.; Demircan, G.; Kilic, A. Effects of Nano Graphene and Nano Hexagonal Boron Nitride on the Thermal and Structural Properties of Fatty Acid Based Green Eutectic PCM. *J. Clust. Sci.* **2025**, *37*, 8. [CrossRef]
18. Morita, S.I.; Haniu, T.; Takai, K.; Yamada, T.; Hayamizu, Y.; Gonda, T.; Horibe, A.; Haruki, N. Thermal Conductivity Estimation of Carbon-Nanotube-Dispersed Phase Change Material as Latent Heat Storage Material. *Int. J. Thermophys.* **2022**, *43*, 70. [CrossRef]
19. Zhao, C.Y.; Tao, Y.B.; Yu, Y.S. Molecular dynamics simulation of nanoparticle effect on melting enthalpy of paraffin phase change material. *Int. J. Heat Mass Transf.* **2020**, *150*, 119382. [CrossRef]
20. Ji, H.; Sellan, D.P.; Pettes, M.T.; Kong, X.; Ji, J.; Shi, L.; Ruoff, R.S. Enhanced thermal conductivity of phase change materials with ultrathin-graphite foams for thermal energy storage. *Energy Environ. Sci.* **2014**, *7*, 1185–1192. [CrossRef]
21. Szatkowska, M.; Szatkowski, P.; Suchorowiec, K.; Radomska, E.; Pielichowska, K. Carbon Black–Enhanced Polyethylene Wax Phase Change Materials for Efficient Photothermal Energy Conversion and Storage in Mobile Heating Systems. *Energies* **2026**, *19*, 1162. [CrossRef]
22. Cheng, G.; Wang, X.; He, Y. 3D graphene paraffin composites based on sponge skeleton for photo thermal conversion and energy storage. *Appl. Therm. Eng.* **2020**, *178*, 115560. [CrossRef]
23. Tang, Q.; Sun, J.; Yu, S.; Wang, G. Improving thermal conductivity and decreasing supercooling of paraffin phase change materials by n-octadecylamine-functionalized multi-walled carbon nanotubes. *RSC Adv.* **2015**, *4*, 36584–36590. [CrossRef]
24. Kuziel, A.W.; Dzido, G.; Turczyn, R.; Jędrysiak, R.G.; Kolanowska, A.; Tracz, A.; Zięba, W.; Cyganiuk, A.; Terzyk, A.P.; Boncel, S. Ultra-long carbon nanotube-paraffin composites of record thermal conductivity and high phase change enthalpy among paraffin-based heat storage materials. *J. Energy Storage* **2021**, *36*, 102396. [CrossRef]
25. Rathgeber, C. *Properties of Phase Change Materials (PCM) in the Lab Environment and under Application Conditions*; IEA SHC Task 58/Annex 33 Subtask 3P, Deliverable D3P1; International Energy Agency Solar Heating and Cooling Programme: Copenhagen, Denmark, 2021.
26. Rubitherm Technologies GmbH. *Technical Data Sheet: RT80HC (English Version)*; Techdata_-RT80HC_EN_20102023; Rubitherm Technologies GmbH: Berlin, Germany, 2023.
27. Varma-nair, M.; Wunderlich, B. Heat capacity and other thermodynamic properties of linear macromolecules X. Update of the ATHAS 1980 Data Bank. *J. Phys. Chem. Ref. Data* **1991**, *20*, 349–404. [CrossRef]
28. Toda, A.; Tomita, C.; Hirosaka, M. Temperature Modulated DSC of Irreversible Melting of Nylon 6 Crystals. *J. Therm. Anal. Calorim.* **1998**, *54*, 623–635. [CrossRef]
29. Righetti, M.C. Crystallization of polymers investigated by temperature-modulated DSC. *Materials* **2017**, *10*, 442. [CrossRef]
30. Li, M.; Guo, Q.; Nutt, S. Carbon nanotube/paraffin/montmorillonite composite phase change material for thermal energy storage. *Sol. Energy* **2017**, *146*, 1–7. [CrossRef]
31. Liu, P.; Gu, X.; Bian, L.; Cheng, X.; Peng, L.; He, H. Thermal Properties and Enhanced Thermal Conductivity of Capric Acid/Diatomite/Carbon Nanotube Composites as Form-Stable Phase Change Materials for Thermal Energy Storage. *ACS Omega* **2019**, *4*, 2964–2972. [CrossRef]

32. Sarı, A.; Biçer, A.; Hekimoğlu, G. Effects of carbon nanotubes additive on thermal conductivity and thermal energy storage properties of a novel composite phase change material. *J. Compos. Mater.* **2018**, *53*, 2967–2980. [CrossRef]
33. Liu, P.; Gu, X.; Zhang, Z.; Rao, J.; Shi, J.; Wang, B.; Bian, L. Capric Acid Hybridizing Fly Ash and Carbon Nanotubes as a Novel Shape-Stabilized Phase Change Material for Thermal Energy Storage. *ACS Omega* **2019**, *4*, 14962–14969. [CrossRef]
34. Ranjbar, S.; Masoumi, H.; Haghighi Khoshkhoo, R.; Mirfendereski, M. Experimental investigation of stability and thermal conductivity of phase change materials containing pristine and functionalized multi-walled carbon nanotubes. *J. Therm. Anal. Calorim.* **2020**, *140*, 2505–2518. [CrossRef]
35. Liu, S.-H.; Shen, M.-Y.; Kuan, C.-F.; Kuan, H.-C.; Ke, C.-Y.; Chiang, C.-L. Improving Thermal Stability of Polyurethane through the Addition of Hyperbranched Polysiloxane. *Polymers* **2019**, *11*, 697. [CrossRef]
36. Tarrío-Saavedra, J.; López-Beceiro, J.; Naya, S.; Artiaga, R. Effect of silica content on thermal stability of fumed silica/epoxy composites. *Polym. Degrad. Stab.* **2008**, *93*, 2133–2137. [CrossRef]
37. Fredi, G.; Dorigato, A.; Fambri, L.; Pegoretti, A. Wax confinement with carbon nanotubes for phase changing epoxy blends. *Polymers* **2017**, *9*, 405. [CrossRef]
38. Cao, X.; Li, C.; Li, Y.; Tong, Y.; He, G.; Yang, Z. Novel paraffin wax/ultra-high molecular weight polyethylene composite phase change materials modified by carbon nanotubes with excellent combination property. *J. Appl. Polym. Sci.* **2022**, *139*, 51564. [CrossRef]
39. Ma, X.; Liu, H.; Chen, C.; Liu, Y.; Zhang, L.; Xu, B.; Xiao, F. Synthesis of novel microencapsulated phase change material with SnO2/CNTs shell for solar energy storage and photo-thermal conversion. *Mater. Res. Express* **2020**, *7*, 015513. [CrossRef]
40. Al-Kelani, M.; Buthelezi, N. Advancements in medical research: Exploring Fourier Transform Infrared (FTIR) spectroscopy for tissue, cell, and hair sample analysis. *Skin. Res. Technol.* **2024**, *30*, e13733. [CrossRef]
41. Špaldoňová, A.; Havelcová, M.; Lapčák, L.; Machovič, V.; Titěra, D. Analysis of beeswax adulteration with paraffin using GC/MS, FTIR-ATR and Raman spectroscopy. *J. Apic. Res.* **2021**, *60*, 73–83. [CrossRef]
42. Black, T.; Boseley, R.E.; Quirk, A.; Young, K.M.; Lunardi-Baccetto, S.; Muyres, B.D.; Laprairie, R.B.; Howland, J.G. Adult Rat Offspring Exposed to THC during Gestation Exhibit Distinct Biomolecular Changes Identified by X-ray Fluorescence Imaging and Fourier Transform Infrared Spectroscopy in Cortico-Limbic Circuits. *ACS Chem. Neurosci.* **2026**, *17*, 719–739. [CrossRef]
43. Pielichowska, K.; Głowinkowski, S.; Lekki, J.; Biniaś, D.; Pielichowski, K.; Jenczyk, J. PEO/fatty acid blends for thermal energy storage materials. Structural/morphological features and hydrogen interactions. *Eur. Polym. J.* **2008**, *44*, 3344–3360. [CrossRef]
44. Larkin, P.J.; Jackson, A. Interpretation of the Infrared Spectra of Metal-Stearate Salts. *Appl. Spectrosc. Pract.* **2024**, *2*, 1–10. [CrossRef]
45. Filopoulou, A.; Vlachou, S.; Boyatzis, S.C. Fatty acids and their metal salts: A review of their infrared spectra in light of their presence in cultural heritage. *Molecules* **2021**, *26*, 6005. [CrossRef]
46. Mani, G.; LaSalle, C.; Gjerde, M.; Hankins, S.; Chretin, D.; Ornberg, A.; Citrowske, S.; Shulfer, R.; Kamberi, M. Development of an FTIR-Based Method for the Detection of Machining Oil Residues on Metallic Biomaterial Surfaces. In Proceedings of the Society for Biomaterials 2026 Annual Meeting and Exposition, Atlanta, GA, USA, 25–28 March 2026.
47. Zhao, S.; Yuan, A.; Xu, H.; Wei, Z.; Zhou, S.; Xiao, Y.; Jiang, L.; Lei, J. Elevating the Photothermal Conversion Efficiency of Phase-Change Materials Simultaneously toward Solar Energy Storage, Self-Healing, and Recyclability. *Appl. Mater. Interfaces* **2022**, *14*, 29213–29222. [CrossRef]
48. Diao, X.; Li, Y.; Wang, P.; Zhao, Z.; Feng, Y.; Guan, C.; Gao, H.; Zhang, X.; Wang, G. Nickel-Induced Dual Carbon Networks Encapsulating Phase Change Materials for Photothermal Conversion and Storage. *Appl. Mater. Interfaces* **2024**, *16*, 66192–66200. [CrossRef]
49. Chen, X.; Cheng, P.; Tang, Z.; Xu, X.; Gao, H.; Wang, G. Carbon-Based Composite Phase Change Materials for Thermal Energy Storage, Transfer, and Conversion. *Adv. Sci.* **2021**, *8*, 2001274. [CrossRef]
50. Chen, Y.; Ma, Q.; Chen, L.; Wang, X.; Zhao, X.; Bing, N.; Yu, W.; Xie, H. Enhanced light-to-thermal conversion performance of self-assembly carbon nanotube/graphene-interconnected phase change materials for thermal-electric device. *J. Energy Storage* **2023**, *72*, 108387. [CrossRef]
51. Li, S.Y.; Yan, T.; Huo, Y.J.; Pan, W.G. Carbon nanotube/carbon foam thermal-bridge enhancing solar energy conversion and storage of phase change materials. *Mater. Today Sustain.* **2024**, *28*, 100986. [CrossRef]

Disclaimer/Publisher's Note: The statements, opinions and data contained in all publications are solely those of the individual author(s) and contributor(s) and not of MDPI and/or the editor(s). MDPI and/or the editor(s) disclaim responsibility for any injury to people or property resulting from any ideas, methods, instructions or products referred to in the content.